

# VAEL: Bridging Variational Autoencoders and Probabilistic Logic Programming.

Eleonora Misino<sup>\*1</sup>, Giuseppe Marra<sup>†2</sup>, and Emanuele Sansone<sup>‡2</sup>

<sup>1</sup>*DISI, University of Bologna*

<sup>2</sup>*Department of Computer Science, KU Leuven*

## Abstract

We present VAE, a neuro-symbolic generative model integrating variational autoencoders (VAE) with the reasoning capabilities of probabilistic logic (L) programming. Besides standard latent subsymbolic variables, our model exploits a probabilistic logic program to define a further structured representation, which is used for logical reasoning. The entire process is end-to-end differentiable. Once trained, VAE can solve new unseen generation tasks by (i) leveraging the previously acquired knowledge encoded in the neural component and (ii) exploiting new logical programs on the structured latent space. Our experiments provide support on the benefits of this neuro-symbolic integration both in terms of task generalization and data efficiency. To the best of our knowledge, this work is the first to propose a general-purpose end-to-end framework integrating probabilistic logic programming into a deep generative model.

## 1 Introduction

Neuro-symbolic learning has gained tremendous attention in the last few years [4, 10, 34, 3] as such integration has the potential of leading to a new era of intelligent solutions, enabling the integration of deep learning and reasoning strategies (e.g. logic-based or expert systems). Indeed, these two worlds have different strengths that complement each other [32]. For example, deep learning systems, i.e. System 1, excel at dealing with noisy and ambiguous high dimensional raw data, whereas reasoning systems, i.e. System 2, leverage relations between symbols to reason and to generalize from a small amount of training data. While a lot of effort has been devoted to devising neuro-symbolic methods in the discriminative setting [49, 69, 51], less attention has been paid to the generative counterpart. A good neuro-symbolic framework should be able to leverage a small amount of training data, acquire the knowledge by learning a symbolic representation and generate data based on new forms of high-level reasoning. For example, let us consider a task where a single image of multiple handwritten numbers is labeled with their sum. Common generative approaches, like VAE-based models, have a strong connection between the latent representation and the label of the training task [37, 31]. Consequently, when considering new generation tasks that go beyond the simple addition, they have to be retrained on new data.

---

<sup>\*</sup>eleonora.misino2@unibo.it

<sup>†</sup>giuseppe.marra@kuleuven.be

<sup>‡</sup>emanuele.sansone@kuleuven.be

In this paper, we tackle the problem by providing a true neuro-symbolic solution, named VAEL. In VAEL the latent representation is not directly linked to the label of the task, but to a set of newly introduced symbols, i.e. logical expressions. Starting from these expressions, we use a *probabilistic logic program* to deduce the label. Importantly, the neural component only needs to learn a mapping from the raw data to this new symbolic representation. In this way, the model only weakly depends on the training data and can generalize to new generation tasks involving the same set of symbols. Moreover, the reasoning component offers a strong inductive bias, which enables a more data efficient learning.

The paper is structured as follows. In Section 2, we provide a brief introduction to probabilistic logic programming and to generative models conditioned on labels. In Section 3, we present the VAEL model together with its inference and learning strategies. Section 4 shows our experiments, while Section 5 places our model in the wider scenario of multiple related works. Finally, in Section 6, we draw some conclusions and discuss future directions.

## 2 Preliminaries

### 2.1 Probabilistic Logic Programming

A *logic program* is a set of *definite clauses*, i.e. expressions of the form  $h \leftarrow b_1 \wedge \dots \wedge b_n$ , where  $h$  is the *head literal* or conclusion, while the  $b_i$  are *body literals* or conditions. Definite clauses can be seen as computational rules: IF all the body literals are true THEN the head literal is true. Definite clauses with no conditions ( $n = 0$ ) are *facts*. In first-order logic programs, literals take the form  $a(t_1, \dots, t_m)$ , with  $a$  a predicate of arity  $m$  and  $t_i$  are the terms, that is constants, variables or functors (i.e. functions of other terms). Grounding is the process of substituting all the variable in an atom or a clause with constants.

ProbLog [9] lifts logic programs to *probabilistic logic programs* through the introduction of probabilistic facts. Whereas a fact in a logic program is deterministically true, a probabilistic fact is of the form  $p_i :: f_i$  where  $f_i$  is a logical fact and  $p_i$  is a probability. In ProbLog, each ground instance of a probabilistic fact  $f_i$  corresponds to an *independent Boolean random variable* that is true with probability  $p_i$  and false with probability  $1 - p_i$ . Mutually exclusive facts can be defined through *annotated disjunctions*  $p_0 :: f_0; \dots; p_n :: f_n$ . with  $\sum_i p_i = 1$ . Let us denote with  $\mathcal{F}$  the set of all ground instances of probabilistic facts and with  $p$  their corresponding probabilities. Every subset  $F \subseteq \mathcal{F}$  defines a *possible world*  $w_F$  obtained by adding to  $F$  all the atoms that can be derived from  $F$  using the logic program. The probability  $P(w_F; p)$  of such a possible world  $w_F$  is given by the product of the probabilities of the truth values of the probabilistic facts; i.e:

$$P(w_F; p) = \prod_{f_i \in F} p_i \prod_{f_i \in \mathcal{F} \setminus F} (1 - p_i) \quad (1)$$

Two inference tasks on these probabilities are of interest for this paper.

**Success:** The probability of a query atom  $y$ , or formula, also called *success probability of  $y$* , is the sum of the probabilities of all worlds where  $y$  is *True*, i.e.,

$$P(y; p) = \sum_{F \subseteq \mathcal{F}: w_F \models y} P(w_F; p) \quad (2)$$

**Sample with evidence:** Given a set of atoms or formulas  $E$ , the *evidence*, the probability of a world given evidence is:

$$P(w_F|E;p) = \frac{1}{Z} \begin{cases} P(w_F;p) & \text{if } w_F \models E \\ 0 & \text{otherwise} \end{cases} \quad (3)$$

where  $Z$  is a normalization constant. Sampling from this distribution provides only worlds that are coherent with the given evidence.

**Example 1** (Addition of two digits). *Let us consider a setting where images contains two digits that can only be 0 or 1. Consider the following two logical predicates:  $\text{digit}(\text{img}, I, Y)$  states that a given image  $\text{img}$  has a certain digit  $Y$  in position  $I$ , while  $\text{add}(\text{img}, z)$  states that the digits in  $\text{img}$  sum to a certain value  $z$ .*

We can encode the digit addition task in the following program  $T$ :

```
p1::digit(img,1,0); p2::digit(img,1,1).
p3::digit(img,2,0); p4::digit(img,2,1).
```

```
add(img,Z) :- digit(img,1,Y1),
               digit(img,2,Y2),
               Z is Y1 + Y2.
```

In this program  $T$ , the set of ground facts  $\mathcal{F}$  is

$$\{\text{digit}(\text{img}, 1, 0), \text{digit}(\text{img}, 1, 1), \text{digit}(\text{img}, 2, 0), \text{digit}(\text{img}, 2, 1)\}.$$

The set of probabilities  $p$  is  $p = [p_1, p_2, p_3, p_4]$ . The ProbLog program  $T$  defines a probability distribution over the possible worlds and it is parameterized by  $p$ , i.e.  $P(\omega_F;p)$ . Then, we can ask ProbLog to compute the success probability of a query using Equation 2, e.g.  $P(\text{add}(\text{img}, 1))$ ; or sample a possible world coherent with some evidence  $\text{add}(\text{img}, 2)$  using Equation 3, e.g.  $w_F = \{\text{digit}(\text{img}, 1, 1), \text{digit}(\text{img}, 2, 1)\}$ .

## 2.2 Generation Conditioned on Labels

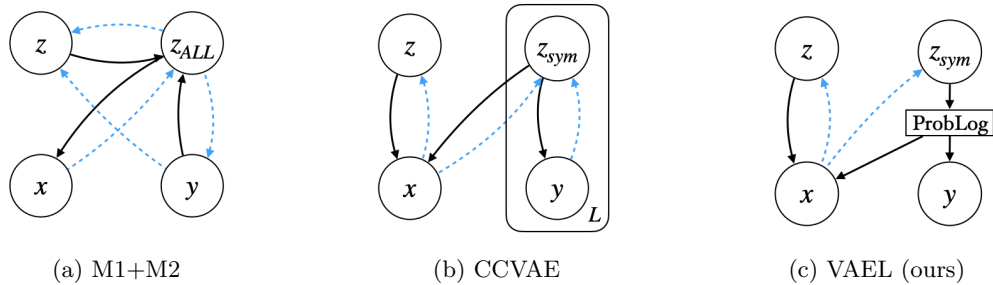


Figure 1: Visual comparison for the probabilistic graphical models of [37] (M1+M2), of [31] (CCVAE) and ours (VAEL). Black arrows refer to the generative model, whereas blue dashed arrows correspond to the inference counterpart.

In this paper, we are interested in generative tasks where we consider both an image  $x$  and a label  $y$ . The integration of supervision into a generative latent variable model has been largely investigated

in the past. For example, the work of [37] proposes an integrated framework between two generative models, called M1 and M2 (cf. Figure 1). Model M1 learns a latent representation for input  $x$ , i.e.  $z_{ALL}$ , which is further decomposed by model M2 into a symbolic and a subsymbolic vector  $y$  and  $z$ , respectively. In this formulation, the generative process of the image is tightly dependent on the label, and therefore on the training task. More recently, another approach, called

CCVAE [31], proposes to learn a representation consisting of two independent latent vectors, i.e.  $z$  and  $z_{sym}$ , and forces the elements of  $z_{sym}$  to have a one-to-one correspondence with the  $L$  elements of  $y$ , thus capturing the rich information of the label vector  $y$  (cf. Figure 1).

However, both the approaches are limited in terms of generation ability as their latent representation encodes information about the training task. This could be problematic when the label  $y$  is only weakly linked to the true symbolic structure of the image. For example, let us consider the addition task in Example 1, where a single image of multiple handwritten numbers is labeled with their sum, e.g.  $x = \mathbf{01}$  and  $y = 1$ . In a generative task where we are interested in creating new images, using only the information of the label  $y$  is not as expressive as directly using the values of the single digits. Moreover, suppose that we want to generate images where the two digits are related by other operations (e.g. subtraction, multiplication, etc). While we still want to generate an image representing a pair of digits, none of the models mentioned before would be able to do it without being retrained on a relabelled dataset. How can we overcome such limitations?

### 3 The VAEL Model

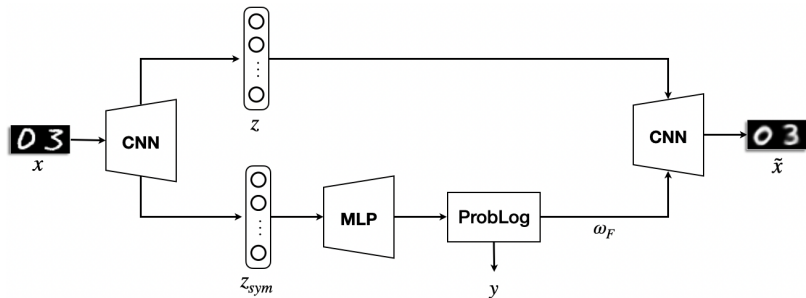


Figure 2: The VAEL model is composed of three components. First, the encoder (**left**) computes an approximated posterior of the latent variables  $\mathbf{z}$  from the image  $x$ . The latent variables are split into two components: a subsymbolic  $z$  and a symbolic  $z_{sym}$ . Second,  $z_{sym}$  is used to parameterize a ProbLog program (**center**). A MLP is used to map the real variables  $z_{sym}$  into the probabilities of the facts in the program. Then, the program is used to compute the label  $y$  and a possible world. Finally, a decoder (**right**) takes both the latent vector  $z$  and the possible world from ProbLog to reconstruct the image  $\tilde{x}$ .

Here, we propose a probabilistic graphical model which enables to unify VAEs with Probabilistic Logic Programming. The graphical model of VAEL (Figure 1) consists of four core variables.  $x \in \mathbb{R}^{H \times W \times C}$  represents the image we want to generate, while  $y \in \{0, 1\}^K$  represents a label, i.e. a symbolic information characterizing the image. The latent variable is split into a symbolic component  $z_{sym} \in \mathbb{R}^N$  and a subsymbolic component  $z \in \mathbb{R}^M$ . Conversely to other VAE frameworks, VAEL does not rely on a one-to-one mapping between  $y$  and  $z_{sym}$ , rather it exploits a probabilistic logic

program to link them. Indeed, the probabilistic facts  $\mathcal{F}$  are used by the ProbLog program  $T$  to compute the actual labels  $y$  and they can encode a more meaningful symbolic representation of the image than  $y$ .

### Generative model.

The generative distribution of VAEL (Figure 1) is factorized in the following way:

$$p_\theta(x, y, \mathbf{z}) = p(x|\mathbf{z})p(y|z_{sym})p(\mathbf{z}) \quad (4)$$

where  $\mathbf{z} = [z_{sym}, z]$  and  $\theta$  are the parameters of the generative model.  $p(\mathbf{z})$  is a standard Gaussian distribution, while  $p(y|z_{sym})$  is the success distribution of the label of the ProbLog program  $T$  (Eq. 2).  $p(x|\mathbf{z})$  is a Laplace distribution with mean value  $\mu$  and identity covariance, i.e.  $Laplace(x; \mu, I)$ . Here,  $\mu$  is a neural network decoder whose inputs are  $z$  and  $\omega_F$ .  $\omega_F$  is sampled from  $P(\omega_F; MLP(z_{sym}))$  (Eq. 1).

**Inference model.** We amortise inference by using an approximate posterior distribution  $q_\phi(\mathbf{z}|x, y)$  with parameters  $\phi$ . Furthermore, we assume that  $\mathbf{z}$  and  $y$  are conditionally independent given  $x$ , thus obtaining  $q_\phi(\mathbf{z}|x, y) = q_\phi(\mathbf{z}|x)$ <sup>1</sup>. This allows us to decouple the latent representation from the training task. Conversely, the other VAE frameworks do not exploit this assumption and have a latent representation that is dependent on the training task.

The overall VAEL model (including the inference and the generative components) is shown in Figure 2.

**Objective Function.** The objective function of VAEL computes an evidence lower bound (ELBO) on the log likelihood of pair  $(x, y)$ , namely:

$$\mathcal{L}(\theta, \phi) = \mathcal{L}_{REC}(\theta, \phi) + \mathcal{L}_Q(\theta, \phi) - \mathcal{D}_{KL}[q_\phi(\mathbf{z}|x)||p(\mathbf{z})] \quad (5)$$

where

$$\mathcal{L}_{REC}(\theta, \phi) = \mathbb{E}_{\mathbf{z} \sim q_\phi(\mathbf{z}|x)}[\log(p(x|\mathbf{z}))], \quad \mathcal{L}_Q(\theta, \phi) = \mathbb{E}_{z_{sym} \sim q_\phi(z_{sym}|x)}[\log(p(y|z_{sym}))].$$

Note that we omit the dependence on  $\omega_F$  in the objective, thanks to an equivalence described in the extended derivation (see Appendix A).

The objective is used to train VAEL in an end-to-end differentiable manner, thanks to the Reparametrization Trick [36] at the level of the encoder  $q_\phi(\mathbf{z}|x)$  and the differentiability of the ProbLog inference, which is used to compute the success probability of a query and sample a world.

In Appendix B we report VAEL training algorithm (Algorithm 1) along with further details on the training procedure.

## 3.1 Downstream Applications

**Label Classification.** Given  $x$  we use the encoder to compute  $z_{sym}$  and by using the MLP we compute the probabilities  $p = MLP(z_{sym})$ . Then, we can predict labels by computing the probability distribution over the labels  $P(y;p)$ , as defined in Eq. 2, and sampling  $y \sim P(y;p)$ . This process subsumes the DeepProbLog framework [49].

<sup>1</sup>We use a Gaussian distribution with a mean parameterized by the encoder network and identity covariance

**Image Generation.** We generate images by sampling  $\mathbf{z} = [z_{sym}, z]$  from the prior distribution  $\mathcal{N}(0, 1)$  and a possible world  $\omega_F$  from  $P(\omega_F; p)$ . The distribution over the possible worlds  $P(\omega_F; p)$  is computed by relying on ProbLog inference starting from the facts probabilities  $p = MLP(z_{sym})$ .

**Conditional Image Generation.** As described in Section 2.1, ProbLog inference allows us also to *sample with evidence*. Thus, once sampled  $\mathbf{z}$  from the prior, we can (i) compute  $p = MLP(\hat{z}_{sym})$ , then (ii) compute the conditional probability  $P(\omega_F | E; p)$ , (iii) sampling  $\omega_F \sim P(\omega_F | E; p)$  and (iv) generate an image consistent with the evidence  $E$ .

**Task Generalization** As we have seen, VAE factorizes the generation task into two steps: (i) generation of the world  $\omega_F$  (e.g. the digits labels); (ii) generation of the image given the world. Whereas the second step requires to be parameterized by a black-box model (e.g. a convolutional neural network), the generation of a possible world  $\omega_F$  is handled by a symbolic generative process encoded in the ProbLog program  $T$ . Thus, once trained VAE on a specific symbolic task (e.g. the addition of two digits), we can generalize to any novel task that involves reasoning with the same set of probabilistic facts by simply changing the ProbLog program accordingly (e.g. we can generalize to the multiplication of two integers). To the best of our knowledge, such a level of task generalization cannot be achieved by any other VAE frameworks.

## 4 Experiments

In this Section, we validate our approach on the four downstream applications by creating two different datasets.

**2digit MNIST dataset.** We create a dataset of 64,400 images of two digits taken from the MNIST dataset [40]. We use 65%, 20%, 15% splits for the train, validation and test sets, respectively. Each image in the dataset has dimension  $28 \times 56$  and is labelled with the sum of the two digits. The dataset contains a number of images similar to the standard MNIST dataset. However, it is combinatorial in nature, making any task defined on it harder than its single-digit counterpart.

**Mario dataset.** We create a dataset containing 6,720 images of two consequent states of a  $3 \times 3$  grid world where an agent can move by one single step (diagonals excluded). Each image has dimension  $100 \times 200$  and is labelled with the move performed by the agent. For example, the image in Figure 3 has label **down**. We use 70%, 20%, 10% splits for the train, validation and test sets, respectively.



Figure 3: Example of *Mario* dataset image. The  $3 \times 3$  grid world (green area) is surrounded by a frame (bricks).

In order to evaluate our approach, we rely on a *reconstruction loss* ( $m_{REC}$ ) in terms of data log-likelihood and two accuracies, *predictive* ( $m_{CLASS}$ ) and *generative* ( $m_{GEN}$ ). Regarding the *predictive accuracy*, we measure the predictive ability of the model as the classification accuracy on the true labels (the *addition* of the two digits for *2digit MNIST* dataset, and the *move* for *Mario* dataset). It is worth mentioning that, for *2digit MNIST* dataset, such accuracy cannot be directly compared with standard values for the single-digit MNIST, as the input space is different: the correct classification of an image requires both the digits to be correctly classified. The *generative accuracy* is assessed by using an independent classifier for each dataset. For *2digit MNIST* dataset, the classifier is trained to classify single digit value; while

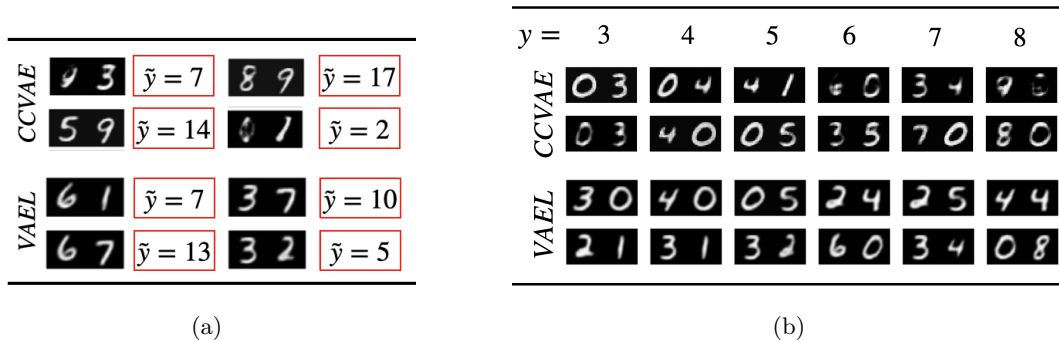


Figure 4: Examples of generation (a) and conditional generation (b) for VAE and CCVAE on *2digit MNIST* dataset. In (b) in each column the generation is conditioned on a different label  $y$ .

for the *Mario* dataset, the classifier learns to identify the agent’s position in a single state. The evaluation process for the generative ability can be summarized as: (i) jointly generate the image and the label  $\tilde{y}$ ; (ii) split the image into two sub-images and (iii) classify them independently; (iv) finally, for *2digit MNIST* dataset, we sum together the outputs of the classifier and we compare the resulting addition with the generated label  $\tilde{y}$ ; while for *Mario Dataset*, we verify whether the classified agent’s positions are consistent with the generated label  $\tilde{y}$ .

In the following tasks, we compare VAE against CCVAE [31] when possible. The source code and the datasets are available at <https://github.com/ElMisi/VAEL> under MIT license. Further implementation details can be found in Appendix D.

**Label Classification.** In this task, we want to predict the correct label given the input image, as measured by the predictive accuracy  $m_{CLASS}$ . Both VAE and CCVAE use an encoder to map the input image to a latent vector  $z_{sym}$ . VAE uses ProbLog inference to predict the label  $y$ . In contrast, CCVAE relies on the distribution  $p(y|z_{sym})$ , which is parameterized by a neural network. As shown in Table 1, CCVAE and VAE achieve comparable predictive accuracy in *Mario* dataset. However, VAE generalizes better than CCVAE in *2digit MNIST* dataset. The reason behind this performance gap is due to the fact that the *addition* task is combinatorial in nature and CCVAE would require a larger number of training samples in order to solve it. We further investigate this aspect in the *Data efficiency* experiment.

**Image Generation.** We want to test the performance when generating both the image and the label. VAE generates both the image and the label  $\tilde{y}$  starting from the sampled latent vector  $\mathbf{z} \sim \mathcal{N}(0, 1)$ . Conversely, CCVAE starts by sampling the label  $\tilde{y}$  from its prior, then proceeds by sampling the latent vector from  $p(\mathbf{z}|\tilde{y})$ , and finally generates the new image. Figure 4a shows some random samples for both models for *2digit MNIST* dataset. The pairs drawn by VAE are well defined, while CCVAE generates more ambiguous digits (e.g., the 1 resembles a 0, the 4 may be interpreted as a 9, and so on). This ambiguity makes it harder for the classifier network to distinguish among the digits during the evaluation process, as confirmed by the quantitative results in Table 1, where VAE outperforms CCVAE in terms of generative ability. Regarding *Mario* dataset (Figure 5a), VAE is able to generate data-like images, where the background is preserved from one state to the subsequent one (additional results can be found in Appendix E). Conversely, CCVAE fails the generation task: although it correctly generates the background, it is not able to draw the

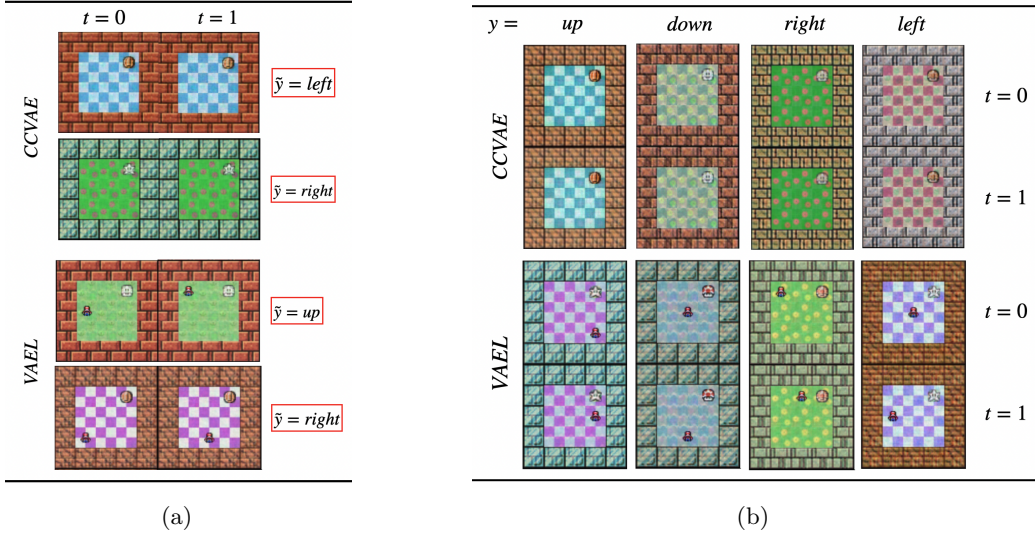


Figure 5: Examples of generation (a) and conditional generation (b) for VAE and CCVAE on *Mario* dataset. In (b) in each column the generation is conditioned on a different label  $y$ .

agent. This is also supported by the disparity in the reconstructive ability, as reported in Table 1. In *Mario* dataset, this is due to a systematic error in which CCVAE focuses only on reconstructing the background, thus discarding the small portion of the image containing the agent, as shown in Figures 5a, 5b and in Appendix E. The difference in performance between CCVAE and VAE lies in the fact that for each label there are many possible correct images. For example, in the *Mario* dataset, there are 6 possible pairs of agent’s positions that correspond to the label `left`. Our probabilistic logic program explicitly encodes the digits value or the single agent’s positions in its probabilistic facts, and uses the variable  $z_{sym}$  to compute their probabilities. On the contrary, CCVAE is not able to learn the proper mapping from the digits value or the agent’s positions to the label, but it can learn to encode only the label in the latent space  $z_{sym}$ .

**Conditional Image Generation.** In this task, we want to evaluate also the conditional generation ability of our approach. In Figures 4b and 5b we report some qualitative results for both VAE and CCVAE (additional results can be found in Appendix E). As it can be seen in 4b, VAE always generates pairs of digits coherent with the evidence, showing also a variety of combinations. Conversely, some of the pairs generated by CCVAE do not sum to the desired value. Regarding *Mario* dataset (Figure 5b), VAE generates pairs of states coherent with the evidence, and with different backgrounds that are preserved from one state to the subsequent one. On the contrary, CCVAE is not able to draw the agent in the generated images, thus failing the task. The reason lies, again, in the task complexity, that VAE reduces by relying on its probabilistic logic program.

**Task Generalization.** We define several novel tasks to evaluate the task generative ability of VAE. For *2digit MNIST* dataset, we introduce the *multiplication*, *subtraction* and *power* between two digits, while for *Mario* dataset we define two shortest paths (*up priority*, i.e. `up` always first, and one with *right priority*, i.e. `right` always first). To the best of our knowledge, such a level of task generalization cannot be achieved by any existing VAE framework. On the contrary, in VAE, we can generalize by simply substituting the ProbLog program used for the training task with the

Table 1: Reconstructive, predictive and generative ability of VAEL and CCVAE. We use repeated trials to evaluate both the models on a test set of 10K images for *2digit MNIST* dataset and 1344 images for *Mario* dataset.

Dataset	Model	$m_{REC}(\downarrow)$	$m_{CLASS}(\uparrow)$	$m_{GEN}(\uparrow)$
<i>2digit MNIST</i>	CCVAE	$1549 \pm 2$	$0.5284 \pm 0.0051$	$0.5143 \pm 0.0157$
	VAEL	<b><math>1542 \pm 3</math></b>	<b><math>0.8477 \pm 0.0178</math></b>	<b><math>0.7922 \pm 0.0350</math></b>
<i>Mario</i>	CCVAE	$43461 \pm 209$	<b><math>1.0 \pm 0.0</math></b>	$0.0 \pm 0.0$
	VAEL	<b><math>42734 \pm 246</math></b>	<b><math>0.977 \pm 0.0585</math></b>	<b><math>0.8135 \pm 0.2979</math></b>

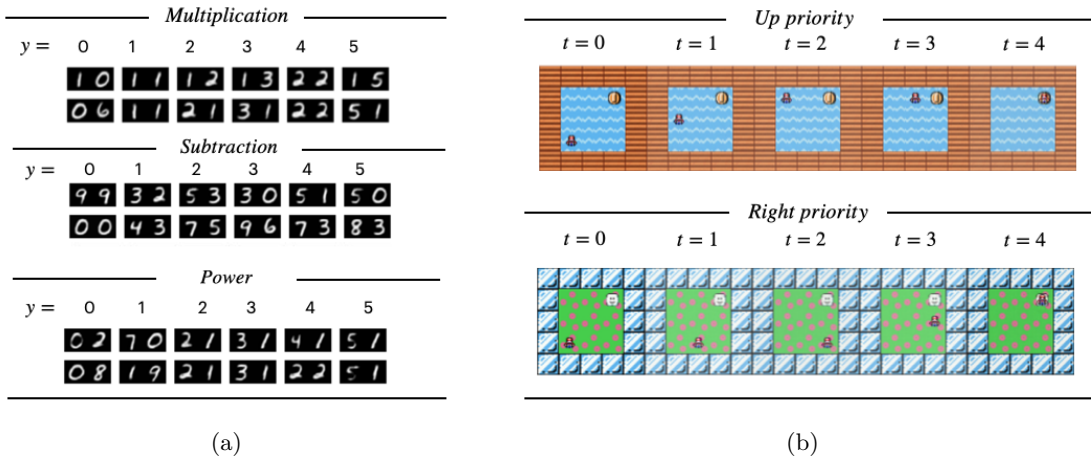


Figure 6: Examples of the generation ability of VAEL in previously unseen tasks for *2digit MNIST* dataset (a) and *Mario* dataset (b).

program for the desired target task, without re-training the model. In Figure 6, we report qualitative results: in 6a, the generation is conditioned on a different label  $y$  referring to the corresponding mathematical operation between the first and second digit; in 6b, the model is asked to generate a trajectory starting from the initial image ( $t = 0$ ) and following the shortest path using an *up priority* or a *right priority*.

In all the novel tasks of *2digit MNIST* dataset (Figure 6a), VAEL generates pairs of numbers consistent with the evidence, and it also shows a variety of digits combinations by relying on the probabilistic engine of ProbLog. This should not surprise. In fact, in all these tasks, the decoder takes as input a possible world, i.e., a specific configuration of the two digits. Therefore, the decoder is agnostic to the specific operation, which is entirely handled by the symbolic program. For this reason, VAEL can be seamlessly applied to all those tasks that require the manipulation of two digits. The same reasoning can be extended to *Mario* novel tasks (Figure 6b), where VAEL generates subsequent states consistent with the shortest path, while preserving the background of the initial state ( $t = 0$ ) thanks to the clear separation between the subsymbolic and symbolic latent components. Additional results can be found in Appendix E.

**Data Efficiency.** In this task, we want to verify whether the use of a logic-based prior helps the

learning in contexts characterized by data scarcity. To this goal, we define different training splits of increasing size for the *addition* task of *2digit MNIST* dataset. In particular, the different splits range from 10 up to 100 images per pair of digits. The results (Figure 13 in Appendix F) show that VAEL outperforms the baseline for all the tested sizes. In fact, with only 10 images per pair, VAEL already performs better than CCVAE trained with 100 images per pair. When considering 10 images per pair, the discriminative and generative accuracies of VAEL are  $0.445 \pm 0.057$  and  $0.415 \pm 0.0418$ , whereas CCVAE trained on 100 images per pair has a discriminative and generative accuracy of  $0.121 \pm 0.006$  and  $0.284 \pm 0.006$  respectively. The reason behind this disparity is that the logic-based prior helps the neural model in properly structuring the latent representation, so that one part can easily focus on recognizing individual digits and the other on capturing the remaining information in the scene. Conversely, CCVAE needs to learn how to correctly model very different pairs that sum up to the same value. We further investigate the performance gap between CCVAE and VAEL by running an identical experiment in a simplified dataset with only three possible digits values: 0, 1 and 2. The goal is to train CCVAE on a much larger number of images per pair, which is impractical in the 10-digits setting, due to the combinatorial nature of the task. Additional details can be found in Appendix F.

## 5 Related Work

**Controlled image generation.** We distinguish between generative models based on text descriptions and generative models based on scene graphs. Regarding the first category, substantial effort has been devoted to devising strategies able to generate images with control (i) on object properties/attributes (e.g. shape, color, texture of objects) [57, 58, 70, 71, 13], (ii) on spatial relations between multiple objects (e.g. object A is below object B) [50, 54, 24, 46], (iii) or both [55]. Our framework is related to these works as considering the problem of generation in a relational setting. Differently from them, we use probabilistic logic programming to encode first-order logical knowledge and to perform reasoning over this knowledge. This comes with the advantage that we can generalize to out-of-distribution relations, which consists of both the composition of previously seen relations (e.g. the multiplication can be composed by using the sum in the domain of natural numbers) and new relations (e.g. the subtraction cannot be composed by using the sum in the domain of natural numbers). Regarding the second category, scene graphs are used as an alternative to text descriptions to explicitly encode relations, such as spatial relations between objects [30, 1, 22, 42, 52, 23, 25, 6]. While related, our approach differs from these last as logical programs are more expressive and allow a more general reasoning than scene graphs alone.

**Unsupervised scene decomposition** We distinguish between object-oriented, part-oriented and hierarchical approaches. The first category attempts to learn individual object representations in an unsupervised manner and to reconstruct the original image or the subsequent frame (in the case of sequential data) from these representations. Several approaches have been proposed, based on scene-mixtures [19, 63, 5, 20, 14, 47, 38, 62], spatial attention models [21, 15, 8] and their corresponding combination [45, 29]. In the second category, a scene with an object is decomposed into its constituent parts. Specifically, an encoder and a decoder are used to decompose an object into its primitives and to recombine them to reconstruct the original object, respectively. Several approaches have been proposed for generating 3D shapes [65, 41, 72, 26, 33, 11] and for inferring the compositional structure of the objects together with their physical interactions in videos [68, 43, 17]. These approaches focus on learning the part-whole relationships of object either by using pre-segmented parts or by using motion cues. Last but not least, there has been recent effort focusing on integrating the previous two categories, thus learning to decompose a scene into both its objects

and their respective parts, the so called hierarchical decomposition [59, 12]. Our work differs in several aspects and can be considered as an orthogonal direction. First of all, we consider static images and therefore we do not exploit temporal information. Secondly, we do not provide any information about the location of the objects or their parts and use a plain autoencoder architecture to discover the objects. Therefore, we could exploit architectural advances in unsupervised scene decomposition to further enhance our framework. However, this integration is left to future investigation. Finally, our model discovers objects in a scene, by leveraging the high-level logical relations among them.

**Neuro-symbolic generation.** This is an emerging area of machine learning as demonstrated by works appeared in the last few years. For example, [28] proposes a generative model based on a two-layered latent representation. In particular, the model introduces a global sub-symbolic latent variable, capturing all the information about a scene and a symbolic latent representation, encoding the presence of an object, its position, depth and appearance. However, the model is limited in the form of reasoning, as able to generate images with objects fulfilling only specific spatial relations. In contrast, our model can leverage a logical reasoning framework and solve tasks requiring to manipulate knowledge to answer new generative queries.

There are two recent attempts focusing on integrating generative models with probabilistic programming [16, 18], where reasoning is limited to spatial relationships of (parts of) the image. Moreover, [18] is a clear example of the difficulty of integration the symbolic and the perceptual module. In contrast, our work provides a unified model which can learn to generate images while perform logical reasoning at the same time.

To the best of our knowledge, the work in [60] represents the first attempt to integrate a generative approach with a logical framework. However, the work differs from ours in several aspects. Firstly, the authors propose a model for an image completion problem on MNIST and it is unclear how the model can be used in our learning setting and for generating images in the presence of unseen queries. Secondly, the authors propose to use sum-product networks as an interface between the logical and the neural network modules. In contrast, we provide a probabilistic graphical model which compactly integrates the two modules without requiring any additional network. Thirdly, we are the first to provide experiments supporting the benefits of such integration both in terms of task generalization and data efficiency.

**Structured priors for latent variable models.** Several structured priors have been proposed in the context of latent variable models. For example, The work in [64] focuses on learning priors based on mixture distributions. [2] uses rejection sampling with a learnable acceptance function to construct a complex prior. The works of [61, 48, 66, 39] consider learning hierarchical priors, [7, 53, 56] introduce autoregressive priors [7]. While structured priors offer the possibility of learning flexible generative models and avoid the local minima phenomenon observed in traditional VAEs, they are quite different from ours. Indeed, our prior disentangles the latent variables to support logical reasoning. Furthermore, the structure of the logic program is interpretable.

## 6 Conclusions and Future Works

In this paper, we presented VAEL, a neuro-symbolic generative model that integrates VAE with Probabilistic Logic Programming. The symbolic component allows to decouple the internal latent representation from the task at hand, thus allowing an unprecedented generalization power. We showcased the potential of VAEL in two image generation benchmarks, where VAEL shows state-

of-the-art generation performance, also in regimes of data scarcity and in generalization to several prediction tasks.

In the future, we plan to improve VAEL by investigating alternative and more scalable semantics for probabilistic programs (e.g. stochastic logic program [67]). Moreover, we plan to apply VAEL to other settings, like structured object generation [44], to showcase the flexibility and expressivity provided by the integration with a probabilistic logic program.

## Acknowledgements

Giuseppe Marra is funded by the Research Foundation-Flanders (FWO-Vlaanderen, GA No 1239422N). Emanuele Sansone is funded by TAILOR, a project funded by EU Horizon 2020 research and innovation programme under GA No 952215. The authors would like to thank Luc De Raedt for supporting this project as an Erasmus Master Thesis, and Federico Ruggeri for his support in the experimental phase.

## References

- [1] Oron Ashual and Lior Wolf. “Specifying Object Attributes and Relations in Interactive Scene Generation”. In: *ICCV*. 2019, pp. 4560–4568.
- [2] Matthias Bauer and Andriy Mnih. “Resampled Priors for Variational Autoencoders”. In: *AISTATS*. 2019, pp. 66–75.
- [3] Yoshua Bengio and Gary Marcus. *AI Debate*. <https://montrealartificialintelligence.com/aidebate/>. 2020.
- [4] Tarek R Besold et al. “Neural-symbolic learning and reasoning: A survey and interpretation”. In: *arXiv preprint arXiv:1711.03902* (2017).
- [5] Christopher P. Burgess et al. “MONet: Unsupervised Scene Decomposition and Representation”. In: *CoRR* (2019).
- [6] Xiaojun Chang et al. “A Comprehensive Survey of Scene Graphs: Generation and Application”. In: *IEEE Trans. Pattern Anal. and Mach. Intell.* (2021), pp. 1–1.
- [7] Xi Chen et al. “Variational Lossy Autoencoder”. In: *ICLR*. 2017.
- [8] Eric Crawford and Joelle Pineau. “Spatially Invariant Unsupervised Object Detection with Convolutional Neural Networks”. In: *AAAI*. 2019, pp. 3412–3420.
- [9] Luc De Raedt, Angelika Kimmig, and Hannu Toivonen. “ProbLog: A Probabilistic Prolog and Its Application in Link Discovery.” In: *IJCAI*. Vol. 7. 2007, pp. 2462–2467.
- [10] Luc De Raedt et al. “From statistical relational to neuro-symbolic artificial intelligence”. In: *IJCAI*. 2020.
- [11] Boyang Deng et al. “CvxNet: Learnable Convex Decomposition”. In: *CVPR*. 2020, pp. 31–41.
- [12] Fei Deng et al. “Generative Scene Graph Networks”. In: *ICLR*. 2021.
- [13] Yilun Du, Shuang Li, and Igor Mordatch. “Compositional Visual Generation and Inference with Energy Based Models”. In: *NeurIPS*. 2020.
- [14] Martin Engelcke et al. “GENESIS: Generative Scene Inference and Sampling with Object-Centric Latent Representations”. In: *ICLR*. 2020.

- [15] S. M. Ali Eslami et al. “Attend, Infer, Repeat: Fast Scene Understanding with Generative Models”. In: *NeurIPS*. 2016, pp. 3225–3233.
- [16] Reuben Feinman and Brenden M. Lake. “Generating New Concepts with Hybrid Neuro-Symbolic Models”. In: *CogSci*. 2020.
- [17] Anand Gopalakrishnan, Sjoerd van Steenkiste, and Jürgen Schmidhuber. “Unsupervised Object Keypoint Learning using Local Spatial Predictability”. In: *ICLR*. 2021.
- [18] Nishad Gothoskar et al. “3DP3: 3D Scene Perception via Probabilistic Programming”. In: *NeurIPS*. 2021.
- [19] Klaus Greff, Sjoerd van Steenkiste, and Jürgen Schmidhuber. “Neural Expectation Maximization”. In: *NeurIPS*. 2017.
- [20] Klaus Greff et al. “Multi-Object Representation Learning with Iterative Variational Inference”. In: *ICML*. 2019, pp. 2424–2433.
- [21] Karol Gregor et al. “DRAW: A Recurrent Neural Network For Image Generation”. In: *ICML*. Vol. 37. 2015, pp. 1462–1471.
- [22] Jiuxiang Gu et al. “Scene Graph Generation With External Knowledge and Image Reconstruction”. In: *CVPR*. 2019, pp. 1969–1978.
- [23] Roei Herzig et al. “Learning Canonical Representations for Scene Graph to Image Generation”. In: *ECCV*. Vol. 12371. 2020, pp. 210–227.
- [24] Seunghoon Hong et al. “Inferring Semantic Layout for Hierarchical Text-to-Image Synthesis”. In: *CVPR*. 2018, pp. 7986–7994.
- [25] Tianyu Hua et al. “Exploiting Relationship for Complex-scene Image Generation”. In: *AAAI*. 2021, pp. 1584–1592.
- [26] Jialei Huang et al. “Generative 3D Part Assembly via Dynamic Graph Learning”. In: *NeurIPS*. 2020.
- [27] Eric Jang, Shixiang Gu, and Ben Poole. “Categorical Reparameterization with Gumbel-Softmax”. In: *ICLR*. 2017.
- [28] Jindong Jiang and Sungjin Ahn. “Generative Neurosymbolic Machines”. In: *NeurIPS*. 2020.
- [29] Jindong Jiang et al. “SCALOR: Generative World Models with Scalable Object Representations”. In: *ICLR*. 2020.
- [30] Justin Johnson, Agrim Gupta, and Li Fei-Fei. “Image Generation From Scene Graphs”. In: *CVPR*. 2018, pp. 1219–1228.
- [31] Tom Joy et al. “Capturing Label Characteristics in VAEs”. In: *ICLR*. 2021.
- [32] Daniel Kahneman. *Thinking, fast and slow*. Macmillan, 2011.
- [33] Kacper Kania, Maciej Zieba, and Tomasz Kajdanowicz. “UCSG-NET - Unsupervised Discovering of Constructive Solid Geometry Tree”. In: *NeurIPS*. 2020.
- [34] Henry Kautz. *The Third AI Summer*. <https://roc-hci.com/announcements/the-third-ai-summer/>. 2020.
- [35] Diederik P. Kingma and Jimmy Ba. “Adam: A Method for Stochastic Optimization”. In: *ICLR*. 2015.
- [36] Diederik P. Kingma and Max Welling. “Auto-Encoding Variational Bayes”. In: *ICLR*. 2014.

- [37] Diederik P. Kingma et al. “Semi-supervised Learning with Deep Generative Models”. In: *NeurIPS*. 2014, pp. 3581–3589.
- [38] Thomas Kipf et al. “Conditional Object-Centric Learning from Video”. In: *CoRR* (2021).
- [39] Alexej Klushyn et al. “Learning Hierarchical Priors in VAEs”. In: *NeurIPS*. 2019, pp. 2866–2875.
- [40] Yann LeCun et al. “Gradient-based learning applied to document recognition”. In: *IEEE* 86.11 (1998), pp. 2278–2324.
- [41] Jun Li et al. “GRASS: generative recursive autoencoders for shape structures”. In: *ACM Trans. Graph.* 36.4 (2017), 52:1–52:14.
- [42] Yikang Li et al. “PasteGAN: A Semi-Parametric Method to Generate Image from Scene Graph”. In: *NeurIPS*. 2019, pp. 3950–3960.
- [43] Yunzhu Li et al. “Causal Discovery in Physical Systems from Videos”. In: *NeurIPS*. 2020.
- [44] Luca Di Liello et al. “Efficient Generation of Structured Objects with Constrained Adversarial Networks”. In: *NeurIPS*. 2020.
- [45] Zhixuan Lin et al. “SPACE: Unsupervised Object-Oriented Scene Representation via Spatial Attention and Decomposition”. In: *ICLR*. 2020.
- [46] Nan Liu et al. “Learning to Compose Visual Relations”. In: *NeurIPS Workshop (CtrlGen)*. 2021.
- [47] Francesco Locatello et al. “Object-Centric Learning with Slot Attention”. In: *NeurIPS*. 2020.
- [48] Lars Maaløe et al. “BIVA: A Very Deep Hierarchy of Latent Variables for Generative Modeling”. In: *NeurIPS*. 2019, pp. 6548–6558.
- [49] Robin Manhaeve et al. “DeepProbLog: Neural Probabilistic Logic Programming”. In: *NeurIPS*. 2018, pp. 3753–3763.
- [50] Elman Mansimov et al. “Generating Images from Captions with Attention”. In: *ICLR*. 2016.
- [51] Pasquale Minervini et al. “Learning reasoning strategies in end-to-end differentiable proving”. In: *ICML*. 2020.
- [52] Gaurav Mittal et al. “Interactive Image Generation Using Scene Graphs”. In: *ICLR Workshop (DeepGenStruct)*. 2019.
- [53] Aäron van den Oord, Oriol Vinyals, and Koray Kavukcuoglu. “Neural Discrete Representation Learning”. In: *NeurIPS*. 2017, pp. 6306–6315.
- [54] Aäron van den Oord et al. “Conditional Image Generation with PixelCNN Decoders”. In: *NeurIPS*. 2016, pp. 4790–4798.
- [55] Aditya Ramesh et al. “Zero-Shot Text-to-Image Generation”. In: *ICML*. Vol. 139. 2021, pp. 8821–8831.
- [56] Ali Razavi, Aäron van den Oord, and Oriol Vinyals. “Generating Diverse High-Fidelity Images with VQ-VAE-2”. In: *NeurIPS*. 2019, pp. 14837–14847.
- [57] Scott E. Reed et al. “Generative Adversarial Text to Image Synthesis”. In: *ICML*. 2016, pp. 1060–1069.
- [58] Scott E. Reed et al. “Learning What and Where to Draw”. In: *NeurIPS*. 2016.
- [59] Sara Sabour et al. “Unsupervised Part Representation by Flow Capsules”. In: *ICML*. Vol. 139. 2021, pp. 9213–9223.

- [60] A. Skryagin et al. “Sum-Product Logic: Integrating Probabilistic Circuits into DeepProbLog”. In: *ICML 2020 Workshop on Bridge Between Perception and Reasoning: Graph Neural Networks and Beyond*. 2020.
- [61] Casper Kaae Sønderby et al. “Ladder Variational Autoencoders”. In: *NeurIPS*. 2016, pp. 3738–3746.
- [62] Aleksandar Stanic, Sjoerd van Steenkiste, and Jürgen Schmidhuber. “Hierarchical Relational Inference”. In: *AAAI*. 2021, pp. 9730–9738.
- [63] Sjoerd van Steenkiste et al. “Relational Neural Expectation Maximization: Unsupervised Discovery of Objects and their Interactions”. In: *ICLR*. 2018.
- [64] Jakub M. Tomczak and Max Welling. “VAE with a VampPrior”. In: *AISTATS*. 2018, pp. 1214–1223.
- [65] Shubham Tulsiani et al. “Learning Shape Abstractions by Assembling Volumetric Primitives”. In: *CVPR*. 2017, pp. 1466–1474.
- [66] Arash Vahdat and Jan Kautz. “NVAE: A Deep Hierarchical Variational Autoencoder”. In: *NeurIPS*. 2020.
- [67] Thomas Winters et al. “DeepStochLog: Neural Stochastic Logic Programming”. In: *UAI, to appear*. 2021.
- [68] Zhenjia Xu et al. “Unsupervised Discovery of Parts, Structure, and Dynamics”. In: *ICLR*. 2019.
- [69] Kexin Yi et al. “Neural-Symbolic VQA: Disentangling Reasoning from Vision and Language Understanding”. In: *NeurIPS*. 2018.
- [70] Han Zhang, Tao Xu, and Hongsheng Li. “StackGAN: Text to Photo-Realistic Image Synthesis with Stacked Generative Adversarial Networks”. In: *ICCV*. 2017, pp. 5908–5916.
- [71] Han Zhang et al. “StackGAN++: Realistic Image Synthesis with Stacked Generative Adversarial Networks”. In: *IEEE Trans. Pattern Anal. Mach. Intell.* 41.8 (2019), pp. 1947–1962.
- [72] Chenyang Zhu et al. “SCORES: shape composition with recursive substructure priors”. In: *ACM Trans. Graph.* 37.6 (2018), 211:1–211:14.

## A ELBO derivation

To derive the ELBO defined in (5) we start from the maximization of the log-likelihood of the input image  $x$  and the class  $y$ , namely

$$\log(p(x, y)) = \log \left( \int p(x, y | \mathbf{z}) d\mathbf{z} \right). \quad (6)$$

Recalling the generative network factorization (4), we can write

$$\log(p(x, y)) = \log \left( \int p_\theta(x | z, z_{sym}) p_\theta(y | z_{sym}) p(z) p(z_{sym}) dz dz_{sym} \right) \quad (7)$$

Then, by introducing the variational approximation  $q_\phi(\mathbf{z}|x)$  to the intractable posterior  $p_\theta(\mathbf{z}|x)$  and applying the factorization, we get

$$\log(p(x, y)) = \log \left( \int \frac{q_\phi(z|x) q_\phi(z_{sym}|x)}{q_\phi(z|x) q_\phi(z_{sym}|x)} p_\theta(x | z, z_{sym}) p_\theta(y | z_{sym}) p(z) p(z_{sym}) dz dz_{sym} \right). \quad (8)$$

We now apply the *Jensen's inequality* to equation (8) and we obtain the lower bound for the log-likelihood of  $x$  and  $y$  given by

$$\int q_\phi(z|x) q_\phi(z_{sym}|x) \log \left( p_\theta(x | z, z_{sym}) p_\theta(y | z_{sym}) \frac{p(z) p(z_{sym})}{q_\phi(z|x) q_\phi(z_{sym}|x)} dz dz_{sym} \right). \quad (9)$$

Finally, by relying on the linearity of expectation and on logarithm properties, we can rewrite equation (9) as

$$\mathbb{E}_{\mathbf{z} \sim q_\phi(\mathbf{z}|x)} [\log(p_\theta(x|\mathbf{z}))] + \mathbb{E}_{z_{sym} \sim q_\phi(z_{sym}|x)} [\log(p_\theta(y|z_{sym}))] + \mathbb{E}_{\mathbf{z} \sim q_\phi(\mathbf{z}|x)} \left[ \log \left( \frac{p(\mathbf{z})}{q_\phi(\mathbf{z}|x)} \right) \right].$$

The last term is the negative Kullback-Leibler divergence between the variational approximation  $q_\phi(\mathbf{z}|x)$  and the prior  $p(\mathbf{z})$ . This leads us to the ELBO of equation (5), that is

$$\begin{aligned} \log(p(x, y)) &\geq \mathbb{E}_{\mathbf{z} \sim q_\phi(\mathbf{z}|x)} [\log(p_\theta(x|\mathbf{z}))] + \mathbb{E}_{z_{sym} \sim q_\phi(z_{sym}|x)} [\log(p_\theta(y|z_{sym}))] - \mathcal{D}_{KL}[q_\phi(\mathbf{z}|x) || p(\mathbf{z})] \\ &:= \mathcal{L}(\theta, \phi). \end{aligned}$$

In VAEI graphical model (Figure 1c), we omit  $\omega_F$  since we exploit an equivalence relation between the probabilistic graphical models (PGMs) shown in Figure 7. Indeed, the objective for the PGM where  $\omega_F$  is explicit is equivalent to the one reported in the paper. This is supported by the derivation of  $\log p(x, y)$  (Eq. 10), which is equivalent to Eq. (5) in our paper, where the expectation over  $\omega_F$  is estimated through Gumbel-Softmax.

$$\begin{aligned} \log p(x, y) &= \log \int_{z, z_{sym}, \omega_F} q(z, z_{sym} | x) p(x | z, \omega_F) p(y | z_{sym}) p(\omega_F | z_{sym}, y) \frac{p(z, z_{sym})}{q(z, z_{sym} | x)} \\ &\geq \int_{z, z_{sym}, \omega_F} q(z, z_{sym} | x) p(\omega_F | z_{sym}, y) \log p(x | z, \omega_F) p(y | z_{sym}) \frac{p(z, z_{sym})}{q(z, z_{sym} | x)} \\ &= \mathbb{E}_{z, z_{sym}, \omega_F} [\log p(x | z, \omega_F)] + \mathbb{E}_{z_{sym}} [\log p(y | z_{sym})] - KL[q(z, z_{sym} | x) || p(z, z_{sym})] \quad (10) \end{aligned}$$

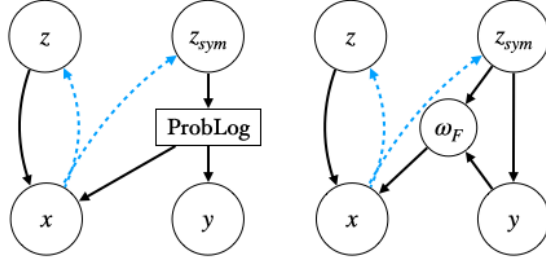


Figure 7: PGM with (left) and without (right) ProbLog box.

## B ELBO estimation and Learning

We estimate the ELBO and its gradients w.r.t. the model parameters using standard Monte Carlo estimates of expectations [36]. Since both  $q_\phi(\mathbf{z}|x)$  and  $p(\mathbf{z})$  are chosen to be Gaussian distributions, the Kullback-Leibler divergence in (5) can be integrated analytically by relying on its closed form. Thus, only the expected reconstruction and query errors  $\mathcal{L}_{REC}(\theta, \phi)$  and  $\mathcal{L}_Q(\theta, \phi)$  require estimation by sampling.

We can therefore define the ELBO estimator as

$$\mathcal{L}(\theta, \phi) \approx \tilde{\mathcal{L}}(\theta, \phi; \epsilon) = \tilde{\mathcal{L}}_{REC}(\theta, \phi; \epsilon) + \tilde{\mathcal{L}}_Q(\theta, \phi; \epsilon) - \mathcal{D}_{KL}[q_\phi(\mathbf{z}|x)||p(\mathbf{z})]. \quad (11)$$

The estimators of  $\mathcal{L}_{REC}$  and  $\mathcal{L}_Q$  can be written as

$$\tilde{\mathcal{L}}_{REC}(\theta, \phi; \epsilon) = \frac{1}{N} \sum_{n=1}^N (\log(p_\theta(x|\hat{\mathbf{z}}^{(n)}))) \quad (12)$$

$$\tilde{\mathcal{L}}_Q(\theta, \phi; \epsilon) = \frac{1}{N} \sum_{n=1}^N (\log(p_\theta(y|\hat{z}_{sym}^{(n)}))) \quad (13)$$

where

$$\begin{aligned} \hat{\mathbf{z}}^{(n)} &= \{\hat{z}^{(n)}, \hat{z}_{sym}^{(n)}\} := \mu(x) + \sigma(x)\epsilon^{(n)}, \\ \epsilon^{(n)} &\sim \mathcal{N}(0, 1). \end{aligned}$$

During the training, we aim at maximizing  $\mathcal{L}(\theta, \phi)$  with respect to both the encoder and the decoder parameters, we therefore need to compute the gradient w.r.t.  $\theta$  and  $\phi$ . Since any sampling operation prevents back-propagation, we need to reparametrize the two sampled variables  $\mathbf{z}$  and  $\omega$ . Due to their nature, we use the well-known *Reparametrization Trick* [36] for the Gaussian  $\mathbf{z}$ , while we exploit the *Categorical Reparametrization with Gumbel-Softmax* [27] for the discrete variable  $\omega$  corresponding to the sampled possible world.

In particular, by defining  $\omega$  as the one-hot encoding of the possible worlds, we have

$$\hat{\omega}_i = \frac{\exp((\log \pi_i + \hat{g}_i)/\lambda)}{\sum_{j=1}^J \exp((\log \pi_j + \hat{g}_j)/\lambda)}, \text{ with } \hat{g}_i \sim \text{Gumbel}(0, 1) \quad (14)$$

where  $J$  is the number of possible worlds (e.g. all the possible pairs of digits), and  $\pi_i$  depends on  $z_{sym}^i$ , which is reparametrized with the Gaussian Reparametrization Trick. In Algorithm 1 we report VAE training algorithm .

---

**Algorithm 1:** VAE Training.

---

**Data:** Set of images  $\mathcal{X}$   
 $\theta, \phi \leftarrow$  Initialization of paramters  
**repeat**  
    *Forward Phase*  
     $x \leftarrow$  Training sample  
     $\mathbf{z} = [z, z_{sym}] \sim q(\mathbf{z} | x)$   
     $p = MLP(z_{sym})$   
     $\omega_F \sim P(\omega_F; p)$   
     $y \sim P(y; p)$   
     $\tilde{x} \sim p(x|z, \omega_F)$   
    *Backward Phase*  
     $\mathbf{g} \leftarrow \nabla_{\theta, \phi} \mathcal{L}(\theta, \phi)$   
     $\theta, \phi \leftarrow$  Update parameters using gradients  $\mathbf{g}$   
**until** convergence of parameters  $(\theta, \phi)$ ;

---

## C Additional supervision for MNIST Task Generalization

During the training on *2digit MNIST* dataset, the model may learn a mapping between symbol and meaning that is logically correct, but different from the desired one. Indeed, the two symbols 1 and 2 used for the left and right positions, respectively, of a handwritten digit in an image are just an assumption. However, VAE may switch the pairs (3, 2) and (2, 3), since they both sum up to 5. This would prevent VAE from generalizing to tasks involving non-commutative operations (i.e. *subtraction* and *power*).

To solve this issue, we simply introduce additional supervision on the digits of very few images (1 image per pair of digits, i.e. 100 images in total) to guide the model toward the desired symbols interpretation. This has to be intended just as an agreement between the model and the human. To include this supervision in the training procedure, we add a regularizer term to the ELBO defined in (5), namely

$$\mathcal{L}_{SUP}(\theta, \phi) := \mathcal{L}(\theta, \phi) + \mathcal{L}_{digits}(\theta, \phi) \quad (15)$$

where

$$\mathcal{L}_{digits}(\theta, \phi) = \mathbb{E}_{z_{sym} \sim q_{\phi}(z_{sym}|x)} [\text{Log}(p_{\theta}(y_{digits}|z_{sym}))]. \quad (16)$$

In equation (16),  $y_{digits}$  refers to the labels over the digits (e.g. for image  we have  $y_{digits} = [0, 1]$ ). Such a digit-level supervision can be easily done by virtue of ProbLog inference, that allows us to retrieve the predicted label of each digit in an image by relying on the query over the digits values.

## D Implementation details

### D.1 VAE

In Tables 2 and 3 we report the architectures of VAE for *2digit MNIST* and *Mario* dataset. For both the datasets we performed a model selection by minimizing the objective function computed on a validation set of 12,000 samples for *2digit MNIST* and 2,016 samples for *Mario*. In all the experiments we trained the model with Adam [35]. The explored hyper-parameters values are reported in Section D.4.

For *2digit MNIST*, the resulting best configuration is: latent space  $z \in \mathbb{R}^M$ ,  $z_{sym} \in \mathbb{R}^N$  with dimension  $M = 8$  and  $N = 15$ ; weights 0.1,  $1 \times 10^{-5}$  and 1.0 for the reconstruction, Kullback-Leibler and classification term of the ELBO respectively; learning rate  $1 \times 10^{-3}$ .

For *Mario*, we obtain: latent space  $z \in \mathbb{R}^M$ ,  $z_{sym} \in \mathbb{R}^N$  with dimension  $M = 30$  and  $N = 18$ ; weights  $1 \times 10^1$ ,  $1 \times 10^1$  and  $1 \times 10^4$  for the reconstruction, Kullback-Leibler and classification term of the ELBO respectively; learning rate  $1 \times 10^{-4}$ .

Table 2: VAE architectures for *2digit MNIST* dataset.

Encoder		Decoder	
Input $28 \times 56 \times 1$ channel image		Input $\in \mathbb{R}^{M+20}$	
$64 \times 1 \times 4 \times 4$ Conv2d stride 2 & ReLU		$(M + 20) \times 256$ Linear layer	
$128 \times 64 \times 4 \times 4$ Conv2d stride 2 & ReLU	$256 \times 128 \times 5 \times 4$ ConvTranspose2d stride 2 & ReLU	$128 \times 64 \times 4 \times 4$ ConvTranspose2d stride 2 & ReLU	
$256 \times 128 \times 4 \times 4$ Conv2d stride 2 & ReLU	$128 \times 64 \times 4 \times 4$ ConvTranspose2d stride 2 & ReLU	$1 \times 64 \times 4 \times 4$ ConvTranspose2d stride 2 & Sigmoid	
$256 \times 2(M + N)$ Linear layer			

MLP & ProbLog	
Input $\in \mathbb{R}^N$	
$N \times 20$ Linear layer & ReLU	
$20 \times 20$ Linear layer	
ProbLog (IN dim: 20, OUT dim: 100)	

Table 3: VAE architectures for *Mario* dataset.

Encoder		Decoder	
Input $200 \times 100 \times 3$ channel image		Input $\in \mathbb{R}^{M+9}$	
$64 \times 3 \times 5 \times 5$ Conv2d stride 2 & SELU		$(M + 9) \times 512$ Linear layer	
$128 \times 64 \times 5 \times 5$ Conv2d stride 2 & SELU	$512 \times 256 \times 5 \times 5$ ConvTranspose2d stride 2 & SELU	$256 \times 128 \times 5 \times 5$ ConvTranspose2d stride 2 & SELU	
$256 \times 128 \times 5 \times 5$ Conv2d stride 2 & SELU	$256 \times 128 \times 5 \times 5$ ConvTranspose2d stride 2 & SELU	$128 \times 64 \times 5 \times 5$ ConvTranspose2d stride 2 & SELU	
$512 \times 256 \times 5 \times 5$ Conv2d stride 2 & SELU	$128 \times 64 \times 5 \times 5$ ConvTranspose2d stride 2 & SELU	$3 \times 64 \times 5 \times 5$ ConvTranspose2d stride 2 & Sigmoid	
$512 \times 2(M + 9)$ Linear layer			

MLP & ProbLog	
Input $\in \mathbb{R}^N$	
$N \times 20$ Linear layer & ReLU	
$20 \times 9$ Linear layer	
ProbLog (IN dim: 18, OUT dim: 24)	

## D.2 CCVAE

In the original paper [31], there was a direct supervision on each single element of the latent space. To preserve the same type of supervision in our two digits addition task, where the supervision is on the sum and not directly on the single digits, we slightly modify the encoder and decoder mapping functions of CCVAE. By doing so, we ensure the correctness of the approach without changing the graphical model. The original encoder function learns from the input both the mean  $\mu$  and the variance  $\sigma$  of the latent space distribution, while the decoder gets in input the latent representation  $\mathbf{z} = \{z_{sym}, z\}$  (please refer to the original paper for more details [31]). In our modified version, the encoder only learns the variance, while the mean is set to be equal to the image label  $\mu = y$ , and the decoder gets in input the label directly  $\mathbf{z}^* := \{y, z\}$ .

In Tables 4 and 5 we report the architectures of CCVAE for *2digit MNIST* and *Mario* dataset. For both the datasets we performed a model selection by minimizing the objective function computed on a validation set of 12,000 samples for *2digit MNIST* and 2,016 samples for *Mario*. In all the experiments we trained the model with Adam [35]. The explored hyper-parameters values are reported in Section D.4.

For *2digit MNIST*, the resulting best configuration is: latent space  $z_{sym} \in \mathbb{R}^N$  with dimension equal to the number of classes  $N = 19$  (due to the one-to-one mapping between  $z_{sym}$  and the label  $y$ ); latent space  $z \in \mathbb{R}^M$  with dimension  $M = 8$ , model objective reconstruction term with weight 0.05, while the other ELBO terms with unitary weights; learning rate  $1 \times 10^{-4}$ .

For *Mario*, we obtain: latent space  $z_{sym} \in \mathbb{R}^N$  with dimension equal to the number of classes  $N = 4$ ; latent space  $z \in \mathbb{R}^M$  with dimension  $M = 300$ , model objective Kullback-Leibler term and classification term with weight  $1 \times 10^4$  and  $1 \times 10^3$  respectively, while the other ELBO terms with unitary weights; learning rate  $1 \times 10^{-4}$ .

Table 4: CCVAE architectures for *2digit MNIST* dataset.

Encoder		Decoder	
Input $28 \times 56 \times 1$ channel image		Input $\in \mathbb{R}^{M+N}$	
64 $\times$ 1 $\times$ 4 $\times$ 4 Conv2d stride 2 & ReLU		$(M + N) \times 256$ Linear layer	
128 $\times$ 64 $\times$ 4 $\times$ 4 Conv2d stride 2 & ReLU	256 $\times$ 128 $\times$ 5 $\times$ 4 ConvTranspose2d stride 2 & ReLU	128 $\times$ 64 $\times$ 4 $\times$ 4 ConvTranspose2d stride 2 & ReLU	
256 $\times$ 128 $\times$ 4 $\times$ 4 Conv2d stride 2 & ReLU	128 $\times$ 64 $\times$ 4 $\times$ 4 ConvTranspose2d stride 2 & ReLU	1 $\times$ 64 $\times$ 4 $\times$ 4 ConvTranspose2d stride 2 & Sigmoid	
256 $\times$ 2(M + N) Linear layer			

Table 5: CCVAE architectures for *Mario* dataset.

Encoder		Decoder	
Input 200 $\times$ 100 $\times$ 3 channel image		Input $\in \mathbb{R}^{M+N}$	
64 $\times$ 3 $\times$ 5 $\times$ 5 Conv2d stride 2 & SELU		$(M + N) \times 512$ Linear layer	
128 $\times$ 64 $\times$ 5 $\times$ 5 Conv2d stride 2 & SELU	512 $\times$ 256 $\times$ 5 $\times$ 5 ConvTranspose2d stride 2 & SELU	256 $\times$ 128 $\times$ 5 $\times$ 5 ConvTranspose2d stride 2 & SELU	
256 $\times$ 128 $\times$ 5 $\times$ 5 Conv2d stride 2 & SELU	256 $\times$ 128 $\times$ 5 $\times$ 5 ConvTranspose2d stride 2 & SELU	128 $\times$ 64 $\times$ 5 $\times$ 5 ConvTranspose2d stride 2 & SELU	
512 $\times$ 256 $\times$ 5 $\times$ 5 Conv2d stride 2 & SELU	128 $\times$ 64 $\times$ 5 $\times$ 5 ConvTranspose2d stride 2 & SELU	3 $\times$ 64 $\times$ 5 $\times$ 5 ConvTranspose2d stride 2 & Sigmoid	
512 $\times$ 2(M + N) Linear layer			

### D.3 Classifiers

In Table 6 we report the architecture of the classifier used to measure the generative ability of VAE and CCVAE for *2digit MNIST* dataset. We trained the classifier on 60,000 MNIST images [40] for 15 epochs with SGD with a learning rate of  $1 \times 10^{-2}$  and a momentum of 0.5, achieving 0.97 accuracy on the test set.

Table 6

MNIST classifier ( <i>2digit MNIST</i> )
Input $28 \times 28 \times 1$ channel image
Linear layer $784 \times 128$ & ReLU
Linear layer $128 \times 64$ & ReLU
Linear layer $64 \times 10$ & LogSoftmax

In Table 7 we report the architecture of the classifier used to measure the generative ability of VAE and CCVAE for *Mario* dataset. We trained the classifier on 9,140 single state images of *Mario* dataset for 10 epochs with Adam [35] optimizer with a learning rate of  $1 \times 10^{-4}$ , achieving 1.0 accuracy on the test set.

Table 7

MNIST classifier ( <i>Mario</i> )
Input $100 \times 100 \times 3$ channels image
Conv layer $5 \times 5 \times 32$ & SELU
Conv layer $5 \times 5 \times 64$ & SELU
Conv layer $5 \times 5 \times 128$ & SELU
Linear layer $2048 \times 9$

### D.4 Optimization

Experiments are conducted on a single Nvidia GeForce 2080ti 11 GB. Training consumed  $\sim 2GB$  for *2digit MNIST* dataset and  $\sim 2.8GB$  for *Mario* dataset, taking around 1 hour and 15 minutes to complete 100 epochs for *2digit MNIST* and 1 hour and 30 minutes to complete 100 epochs for *Mario* dataset. As introduced in the previous sections, we performed a model selection based on ELBO minimization for both the model.

In the following bullet lists,  $lr$  refers to the learning rate,  $z, z_{sym}$  refer to the latent vectors dimensions,  $W_{REC}, W_{KL}, W_Q$  refer to the weights of  $\mathcal{L}_{REC}, \mathcal{D}_{KL}, \mathcal{L}_Q$  terms of VAE objective function, and  $W_{REC}, W_{KL}, W_{q(y|z_{sym})}, W_{q(y|x)}$  refer to the corresponding terms of CCVAE objective function (please refer to the original paper for more details [31]).

For *2digit MNIST* we explore the following values; we repeat the model training 5 times for each configuration.

- VAE
  - $z \in \{8, 9, 10\}$

- $z_{sym} \in \{15, 19\}$
- $lr \in \{0.0001, 0.001\}$
- $W_{REC} \in \{0.0001, 0.001, 0.01, 0.1, 1, 10, 100\}$
- $W_{KL} \in \{0.00001, 0.0001, 0.001\}$
- $W_Q \in \{1, 5\}$

- CCVAE

- $z_{sym} \in \{8, 10, 15, 20, 30\}$
- $lr \in \{0.00001, 0.0001\}$
- $W_{KL} \in \{0.0001, 0.001, 0.01, 0.1, 1, 10, 100\}$
- $W_{REC} \in \{0.01, 0.1, 1, 10, 100\}$
- $W_{q(y|z_{sym})} \in \{0.01, 0.1, 1, 10, 100\}$
- $W_{q(y|x)} \in \{0.01, 0.1, 1, 10, 100\}$

For *Mario* we explore the following values; we repeat the model training 5 times for each configuration.

- VAEL

- $z \in \{20, 25, 30, 35, 40\}$
- $z_{sym} \in \{18, 20\}$
- $lr \in \{0.0001, 0.0005\}$
- $W_{REC} \in \{1, 10\}$
- $W_{KL} \in \{0.1, 1, 10\}$
- $W_Q \in \{1, 100, 10000\}$

- CCVAE

- $z_{sym} \in \{3, 4, 5, 10, 20, 30, 40, 50, 100, 200, 300, 400\}$
- $lr \in \{0.0001, 0.0005\}$
- $W_{KL} \in \{0.0, 0.0001, 0.001, 0.01, 0.1, 1, 10, 100, 1000\}$
- $W_{REC} \in \{1, 10\}$
- $W_{q(y|z_{sym})} \in \{1, 10, 100\}$

–  $W_{q(y|x)} \in \{1, 10, 100, 1000\}$

## E Additional Results

Here we report some additional results for the tasks described in Section 4.

Figures 8 and 9 show additional qualitative results for the *Conditional Image Generation* and *Task Generalization* experiments relative to *2digit MNIST* dataset.

In Figures 10 and 11, we report some additional examples of *Image Generation* and *Task Generalization* for *Mario* dataset. As it can be seen in Figure 11, VAEL is able to generate subsequent states consistent with the shortest path, whatever the agent’s position in the initial state ( $t = 0$ ). Moreover, the model generates states that are consistent with the initial one in terms of background.

Figure 12 shows some examples of image reconstruction for CCVAE. As it can be seen, CCVAE focuses only on reconstructing the background and discards the small portion of the image containing the agent, thus causing the disparity in the reconstructive and generative ability between VAEL and CCVAE (Table 1).

y =	0	1	2	3	4	5	6	7	8	9	10	11	12	13	14	15	16	17	18
CCVAE	00	01	20	03	04	41	00	34	95	95	39	33	95	47	57	96	77	98	99
	00	10	02	03	40	05	35	70	80	09	46	77	66	76	96	67	77	98	99
VAEL	00	01	02	30	40	05	24	25	44	36	55	92	93	58	68	87	88	89	99
	00	10	20	21	31	32	60	34	08	36	19	29	93	67	68	69	79	89	99

Figure 8: Conditional generation for CCVAE and VAEL for *2digit MNIST* dataset. In each column the generation is conditioned on a different sum  $y$  between the two digits.

		Multiplication																	
y =	0	1	2	3	4	5	6	7	8	9	10	12	14	15	16	18	20	21	24
	10	11	12	13	22	15	32	71	81	91	52	34	72	53	28	92	54	73	64
	06	11	21	31	22	51	32	17	24	91	25	34	27	35	82	63	45	37	46
		Subtraction																	
y =	0	1	2	3	4	5	6	7	8	9	-9	-8	-7	-6	-5	-4	-3	-2	-1
	99	32	53	30	51	50	71	92	91	90	23	09	08	29	17	38	26	36	57
	00	43	75	96	73	83	71	70	91	90	01	09	08	07	39	16	59	36	57
		Power																	
y =	0	1	2	3	4	5	6	7	8	9	16	32	64	128	256	512	27	81	243
	02	70	21	31	41	51	61	71	23	91	42	25	43	27	28	83	33	34	35
	08	19	21	31	22	51	61	71	23	91	42	25	82	27	44	83	33	92	35

Figure 9: Examples of the generation ability of VAEL in 3 previously unseen tasks for *2digit MNIST* dataset. In each column the generation is conditioned on a different label  $y$  referring to the corresponding mathematical operation between the first and second digit.

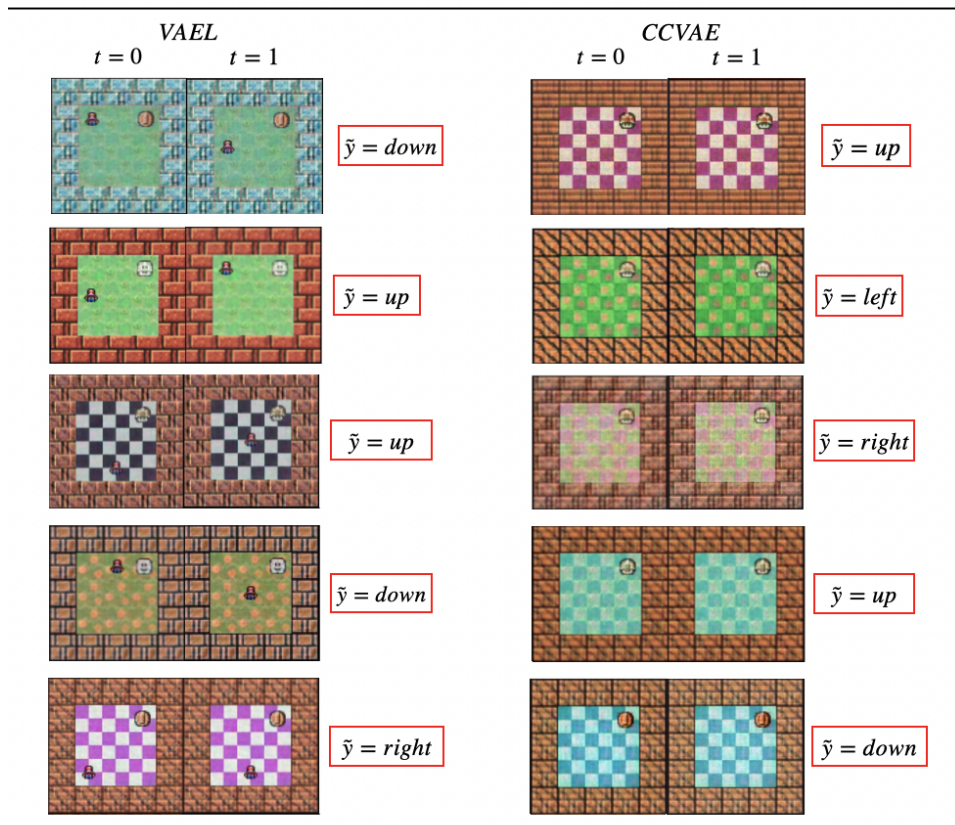


Figure 10: Examples of the generation ability of CCVAE and VAEL for *Mario* dataset.

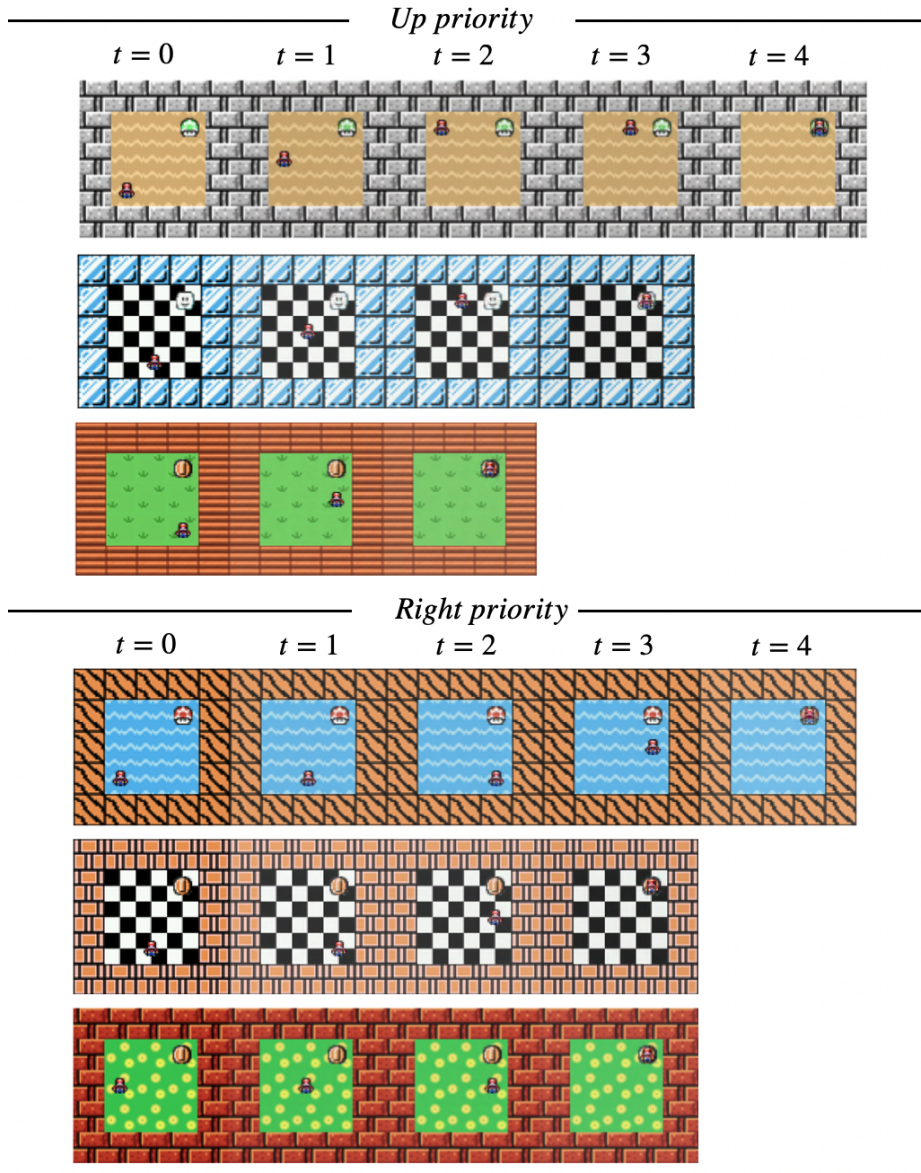


Figure 11: Examples of the generation ability of VAE in previously unseen tasks for *Mario* dataset. In each row, VAE generates a trajectory starting from the initial image ( $t = 0$ ) and following the shortest path using an *up priority* or a *right priority*.

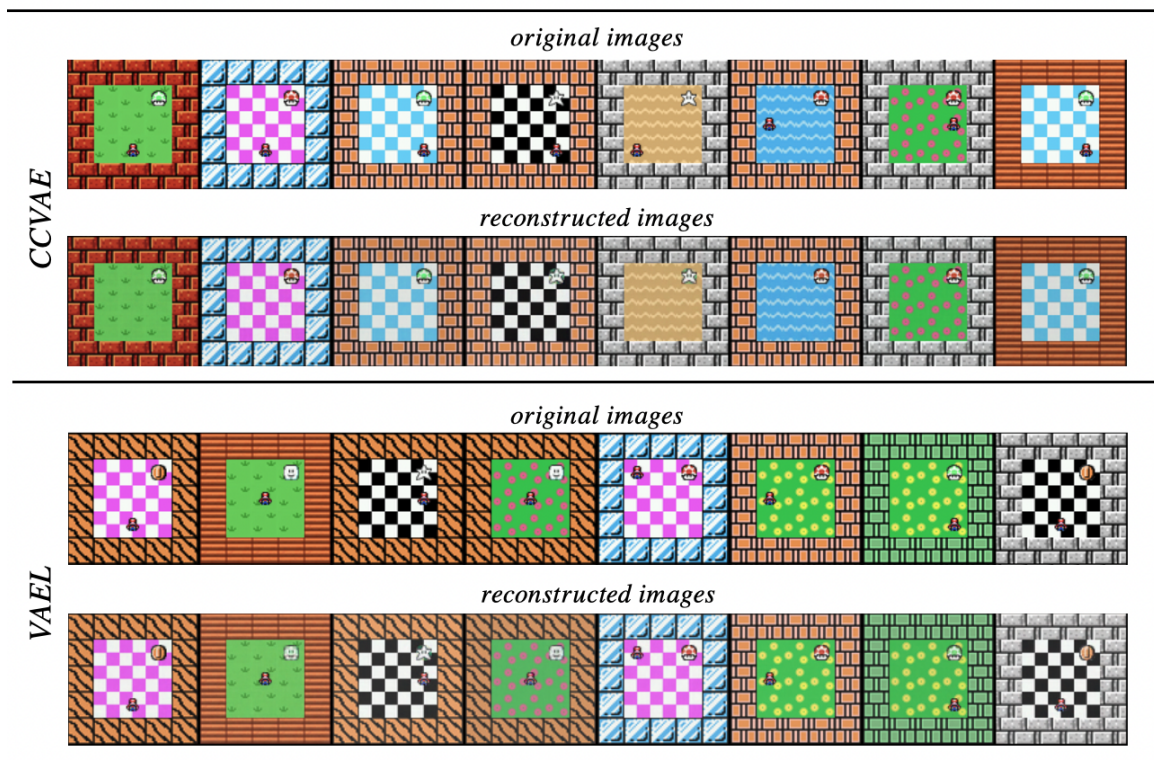


Figure 12: Examples of reconstructive ability of CCVAE and VAE trained on *Mario* dataset.

## F Data Efficiency: simplified setting

We compare VAE and CCVAE discriminative, generative and reconstructive ability when varying the training size of *2digit MNIST* dataset. As it can be seen in Figure 13, VAE outperforms the baseline for all the tested sizes. In fact, with only 10 images per pair VAE already performs better than CCVAE trained with 100 images per pair.

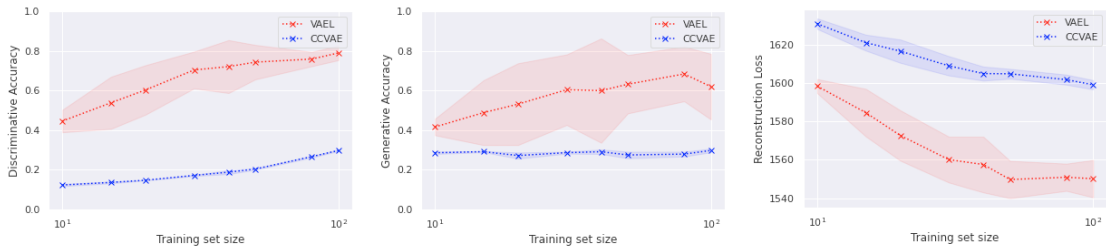


Figure 13: Discriminative, generative and reconstructive ability of VAE (red) and CCVAE (blue) trained in contexts characterized by data scarcity. Both the models are evaluated on the same test set. The training size refers to the number of samples per pair of digits see during the training.

To further investigate the performance gap between CCVAE and VAE in the *Data Efficiency* task 4, we run an identical experiment in a simplified dataset with only three possible digits values: 0, 1 and 2. The goal is to train CCVAE on a much larger number of images per pair, which is impractical in the 10-digits setting, due to the combinatorial nature of the task. The dataset consists of 30,000 images of two digits taken from the MNIST dataset [40]. We use 80%, 10%, 10% splits for the train, validation and test sets, respectively. As for the 10-digits dataset, each image in the dataset has dimension  $28 \times 56$  and is labelled with the sum of the two digits. In Figure 14 we compare VAE and CCVAE discriminative, generative and reconstructive ability when varying the training size. In this simplified setting, CCVAE requires around 2500 images per pair to reach the accuracy that VAE achieves trained with only 10 images per pair.

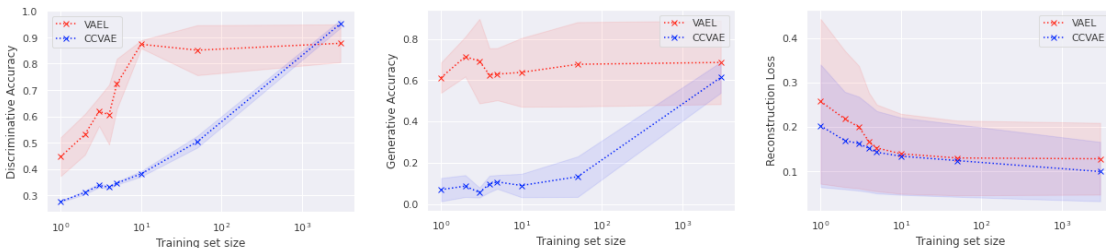


Figure 14: Discriminative, generative and reconstructive ability of VAE (red) and CCVAE (blue) trained in contexts characterized by data scarcity. Both the models are evaluated on the same test set. The training size refers to the number of samples per pair of digits see during the training.